Ous, T. & Arcoumanis, C. (2009). The formation of water droplets in an air-breathing PEMFC. International Journal of Hydrogen Energy, 34(8), pp. 3476-3487. doi: 10.1016/j.ijhydene.2009.02.037

The Formation of Water Droplets in an Air-Breathing PEMFC

T. Ous and C. Arcoumanis

Energy and the Environment Research Centre, School of Engineering & Mathematical Sciences, City University London, United Kingdom

To be submitted to the
International Journal of Hydrogen
2009

Abstract

Air-Breathing Proton Exchange Membrane Fuel Cells (AB-PEMFC) have the potential to supersede lithium ion batteries in portable electronics. However, their water management issue has yet to be resolved to

ensure optimum cell performance and safe system operation. In this paper, the formation of water droplets and their aggregation in the cathode flow channels of an operating AB-PEMFC is investigated by direct visualisation under various operating conditions. The developed optical set-up enables observation of droplet formation on the surface of the membrane from the top and side view of the channels simultaneously. The two orthogonal views reveal that during formation the receding and advancing droplet contact angles are almost identical with values that increase, in a similar trend to the droplet height, with increasing droplet diameter. Water films were able to develop and maintain direct contact with the side-wall of the channels even under the effect of gravitational force. The aggregation of water droplets in the channels was strongly influenced by the change in the air and hydrogen stiochiometry conditions. However, these operating parameters appear to have no significant effect on the water extraction from the channels contrary to load and temperature, where temperature has proved to be the most effective water removal mechanism with minimum reduction in the current density of AB-PEMFC.

Keywords

AB-PEMFC, visualisation, water droplets, contact angle, flow channels, droplet height

1. Introduction

Lithium-ion (Li-ion) batteries may not be the ideal solution to power portable electronic devices after all. They still, and for a long period, suffer from aging also known as shelf life, which causes their performance and charging capacity to decline considerably with time regardless of their usage [1]. The fact that most electronic systems are continuously upgrading to more advanced systems of added functionalities, raises more doubts about whether they are capable of fulfilling the energy needs of this broad and important sector. Meanwhile, Air-Breathing Proton Exchange Membrane Fuel Cells (AB-PEMFC) are receiving more attention as a potential replacement and, in particular, for systems of high energy storage requirements [2]. These passive type cells consume ambient air for their operation through natural free convection; as such, they eliminate the need for air-supply subsystems including compressor, humidifier and other components which minimises the Balance-Of-Plant (BOP) cost and complexity. Their hydrogen-supply subsystem can even be miniaturised by combining it with on-demand micro hydrogen generator/galvanic cell [3].
Although the system cost can be reduced, this may compromise the cell performance. Since the cathode channels are exposed to the atmosphere, the air flow, pressure and temperature will be depending entirely on the ambient conditions which can limit the output power of AB-PEMFC based on the Nernst relationship which relates the cell voltage with the operating pressure and temperature. Therefore, the maximum power density of AB-PEMFC is around 350 mW/cm^2 [4] whereas in conventional PEMFC it is in the range of 566 mW/cm^2 [5].

Prior experimental studies have investigated a number of design issues like dead-end hydrogen mode [6]; micro-flow channels [7]; plastic flow plates [8], anode current collector [9], and cathode open area [10-12] in order to ameliorate the performance and minimise the manufacturing cost of AB-PEMFC. Several numerical models were also developed to identify the optimum cell configurations and operating conditions [13-18]. Most simulations [19-26] were carried out to elucidate the complex and interrelated transport phenomena of ion, heat and mass in AB-PEMFC which provided useful insight into the water formation and membrane hydration state during operation. Furthermore, the water transport mechanism in AB-PEMFC was addressed in [27-30]. In [27], the net water drag coefficient was determined under various operating conditions to optimise the cathode structure through catalyst loading and GDL properties. In [28], different hydrophilic loading mechanisms of the anode catalyst layer were examined, with the aim to improve the water management of AB-PEMFC by achieving proper hydration of the anode and water removal from the cathode. In [27] the use of the ratio between thermal and mass transport resistances was suggested as a tool to monitor the level of hydration/dehydration of the membrane. In addition, [30] identified by varying the current density of the cell three regions of membrane operation: full hydration, partial hydration, and dry-out, and emphasised the vigorous influence of temperature in the transition between those regions. Nevertheless, these studies have not been supported yet by real images of water accumulation in the channels, which has been unsatisfactory for quite sometime.

In the present study, and probably for the first time, the formation of water droplets and their aggregation in the cathode flow channels of AB-PEMFC are visualised under different operating conditions including air stoichiometry, hydrogen stoichiometry, cell temperature, and external load. The advanced optical arrangement achieved by the two CCD cameras permits the capture of two orthogonal views (side and top view images to the channels) of the water droplets and liquid films on the surface of the membrane. In particular, the set-up facilitates measurements of droplet diameter, droplet height, contact angles, and interfacial area with the surface as well as analysis of other relevant phenomena during the formation process while monitoring the polarisation behaviour of AB-PEMFC under natural and forced air convection.

2. Experimental

2.1 System Set-up

Figure 1 shows the schematic of the system which comprises the fuel cell unit (FCU), air fan, hydrogen unit, operation control unit (OCU), data monitoring unit, and visualisation unit. The fuel cell and visualisation units are described in more detail in sections 2.2 and 2.3, respectively. The air fan (Bi-Sonic model: SP802512 H-03) is located close to the opening of the FCU cathode channels to provide a wide range of air velocities (0.057-1.9m/s) for the cell reaction. On the other side of the channels, at the channels exit, a precision anemometer (DANTEC type 54N60) with an accuracy of 5% and a built-in K type humidity sensor (Honeywell HIH-3610) were installed to measure the average air velocity and air humidity in the channels. The fan speed is controlled by the OCU using a variable power supply (Metrix AX-321) which also controls the temperature and electric load across the cell. The hydrogen unit supplies dry hydrogen fuel to the FCU from a cylinder (BOC purity 99.95%) and regulates its pressure and flowrate using a BOC two-stage regulator (model L200-BS4) and a CT Platon flow meter, respectively. The measured data including air velocity, air humidity, operating temperature, and cell voltage and current density are collected in the data monitoring unit via a data acquisition system (National Instrument PCI-6225) and a compatible Labview software.

Figure 1 Schematic diagram of system set-up

2.2 Fuel Cell Unit (FCU)

The FCU uses a Johnson Matthey Membrane Electrode Assembly MEA (Nafion) which has an active area of 25cm^2 and Platinum catalyst loading of 3.5 mgm^{-3}. The MEA is hot pressed with two Gas Diffusion Layers GDL (Toray paper TGP-H-060) on each side and the complete set is sandwiched between anode and cathode aluminium flow plates, as illustrated in Figure 2. The channels of the anode plate are machined in serpentine shapes with a channel width of 1.5 mm, a depth of 1.5 mm, and a length of 655

mm. The cathode flow plate has four straight parallel channels machined-through with lands interconnected by narrow bridges; such design enables optical accessibility to the channels while maintaining the lands attached to the plate. However, the presence of the land-bridges will slightly disturb the air flow in the channels since they contribute by 35% to the total cross sectional area of the channel that is facing the flow. At the channel entrance, the flow will accelerate around the land-bridges causing recirculation zones in regions behind those bridges. The distance between two bridges of the same channel is twelve times larger than their depth and therefore the flow is expected to redevelop along the channel. The width of the cathode flow channels (e.g. 5mm) was made larger than a typical fuel cell channels in order to facilitate the machining of the plate, to minimise the effect of land-bridge in disturbing the air flow in the channel and, above all to allow better visualisation from the two view directions to the channels. This as a consequence would likely to influence the frequency of droplet/droplet interactions and aggregation versus droplet/wall interactions and also increase the ohmic loss of the cell lowering the polarisation performance.

Two holes were drilled on the upper side of the cathode plate to accommodate a thermocouple probe for temperature monitoring and polarisation measurements of the cell (Kelvin electrical connection). A Plexiglass window was mounted on the top of the cathode flow plate whereas a copper heating plate was placed at the back of the anode flow plate to control the operating temperature of the cell. The plates were assembled by fastening 12 screws (12Nm of applied torque) across each side of the end plates.

Figure 2 Fuel Cell Unit (FCU)

2.3 Visualisation Unit

The visualisation unit is equipped with two CCD cameras (Sensi-Cam 12BIT cooled Fast Shutter) mounted on separate bi-directional spindles that provide highly accurate and repeatable positioning in the vertical and the horizontal plane of the FCU, as shown in Figure 3. This arrangement provides the flexibility to observe along the cathode channels the two-sided view, e.g. from the top and side view of the channels. An intensive light source (Schott-Fostec LLC) was positioned to direct light accurately at an angle to the visualisation area on the surface. The recording time of the two cameras was synchronised to avoid delays between the captured images which were saved in workstations1 and 2 for further analysis.

Figure 3 Visualisation unit set-up

2.4 Procedure

Before operating the FCU, a calibration test was conducted to correlate the power supply voltage that

drives the air fan with the air velocity in the cathode flow channels. Four operating parameters including: air stoichiometry, hydrogen stoichiometry, cell temperature, and electric load were examined in separate experiments under ambient room temperature (23C°) and relative humidity of air (RH) of 40%. Between each experiment the air fan was kept running for around 1 hour, without the supply of hydrogen, to extract all liquid water accumulated in the channels and return the membrane state to ambient condition. The operating conditions of those tests are listed in Table 1.

The observation of droplets from the top and side view of the channels proved difficult due to a number of factors. First, the water that is produced at the cathode by the electrochemical reaction of the cell condenses on the upper window of the channels obstructing visual accessibility from the top. In addition, the intensive light source used for flow visualisation also generates extra heat on the surface of the GDL which causes local droplets to evaporate before emerging. Finally, the fact that many droplets appearing in the channels are of similar size makes it extremely hard to identify the same droplet by the two cameras. These issues were addressed by controlling carefully the heat and light conditions of the FCU simultaneously. For the droplet formation test in section (3.1), the images were captured at 30 s intervals whereas for the droplets accumulation test in section (3.2) the corresponding times were set at 5 min intervals. These timings were selected to provide time independency of the phenomena observed.

3. Results and Discussion

3.1 Droplets formation on the surface

The operating conditions of Experiment 1 (Table 1) were selected for droplets augmentation tests. Figure 4 shows images of water droplets on the surface of the GDL during formation at various locations in the channels. The images revealed that droplets emerge spontaneously on the surface in different sizes. This sudden appearance is likely to be associated with the build-up of pressure within the GDL that pushes the water out through local pores instantaneously after reaching water saturation state. Droplets continue to develop on the surface with unsteady increase in diameter until they reach a maximum size where no further enlargement takes place.

The changes in droplet size and contact angle during the operation of AB-PEMFC were measured for a limited number of samples due to the droplets tendency for fast evaporation by superimposing images of droplet boundaries and their interface with the surface using the MatLab program. Droplet boundaries were detected in Matlab using the ‘Canny edge’ detector technique with Gaussian standard deviation value of 3 for improved image quality. Maximum uncertainty of the obtained results was estimated to be around 10% in the case of most blurred images.

Figure 4 Droplet formation on the surface of GDL at various locations in the cathode flow channels

The results in Figure 5 and 6 represent an average value of all conducted test results. It can be estimated from Figure 5 that at each instant of droplet development, at a 30 s intervals, the droplet increases in diameter and height by an average of 60 µm and 55 µm, respectively, giving an overall volumetric increase by around 63 nliter. This droplet formation rate of around 10 µm/min is larger than the one reported for a conventional PEMFC (8 µm/min) [31]. Although the difference between these two values is small but these could be useful data to relate the increase in the current density of AB-PEMFC (~30 mA/cm^2) with the amount of water produced by the reaction. It was also found from the processed images that the point at which the three phases (liquid, air, and membrane) intersect has shifted along the surface by approximately 120 µm during the entire formation period. The droplet would therefore gain an additional interfacial area with the surface of around 0.173 mm^2, thus raising the effect of the adhesive force between them.

The graphs in Figure 6 show the correlations between droplet diameter, height and contact angle during droplet growth on the surface. Both of the droplet height and contact angles are directly proportional to droplet diameter having similar trends with respect to the droplet diameter increase. The dynamic receding and advancing droplet contact angles were measured directly from the side view images of the channels (droplet side profile) using the sessile drop method. Those angles were found almost identical since the shear stress of the air in the channels is relatively low to cause droplet deformation on the side facing the air flow.

The increased in droplet height tends to reduce slightly at larger diameters which maybe caused by the increase in the weight of the enlarged droplet as well as the effect of air flow on a larger droplet surface area that pushes it further into the porous surface. It was also observed that droplet height reduces gradually between consecutive droplet developing stages. The small reduction which can be characterised as droplet ‘Settling’ time maybe related to the pressure difference between the flow channel and the surface that forces the droplet back into the porous media before the next water production period. This phenomenon could not be observed by the vertical visualisation of camera 2 since the top view will only show droplet diameters which remain unchanged.

The deviation of droplet shape on the surface from a perfect circle shape was analysed by superimposing a circle that crosses the horizontal wall with the visualised contact angle into droplet boundary images. The visualised droplet height was found to be larger than a perfect circle. This implies that droplet is deformed in a direction opposite to gravitational force which is likely to be attributed to the adhesive force on the surface that forces the droplets upwards in respect the contact surface.

Figure 5 Images of droplet formation on the surface of GDL during AB-PEMFC operation

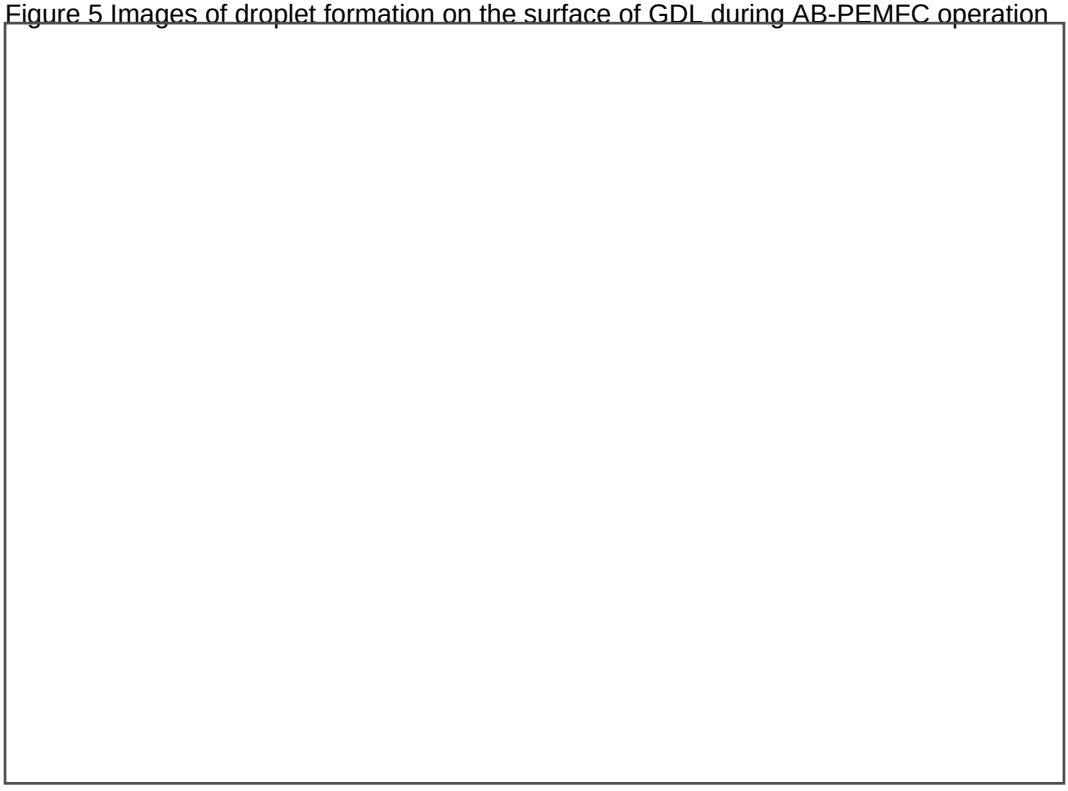

Figure 6 Changes in droplets contact angle and height as a function of the droplet diameter

3.2 Droplets accumulation in the channels

Four operating parameters including air stoichiometry, hydrogen stoichiometry, cell temperature, and electric load were tested in Experiments 2-5 (Table 1) to elucidate their effect into the accumulation of water droplets in the cathode channels and cell polarisation characteristics. Droplets visualisation was carried out by camera 2 (vertical observation) onto the middle flow channels since droplets seemed to appear first on those locations rather than at the entrance or at the exit of the channels.

Effect of air stoichiometry

The effect of air stoichiometry was examined under natural free and forced convection conditions in Experiment 2. Before operating AB-PEMFC, hot wire probe was placed just outside the exit of the air channels at different locations (right wall, centre, left wall) in order to estimate the average air velocity in the channels under different fan speeds. These calibration measurements which assume the average velocity values and flow profile in the channels to be unaffected by the presence of the probe allow calculation of the air stoichiometric ratio. The average air velocity values were converted to mass flow values from the known channel dimensions and the results were divided by the mass air flow required by the cell reaction rate at a current density of 150 mA/cm^2. For example; when the air fan was not in use or at the natural free convection case, the average air velocity in the channels was 57 × 10^{-3} m/s. This velocity value in the flow channel which has a cross sectional area of 4 × 5 mm^2 corresponds to a mass flow ($Mass_{flow}$) of 6.84 × 10^{-2} L/min. The mass flow required by the cell reaction ($Mass_{reacted}$) can be calculated directly from the basic fuel cells air usage equation (air usage = 3.57 × 10^{-7} × total cell current kg.s^{-1}). The total cell current at 150 mA/cm^2 is 3.75 A (e.g. 150 mA/cm^2 × 25 cm^2 of membrane active area). The result of the air usage (13.38 × 10^{-7} kg.s^{-1}) is then multiplied by 60 × 1000 and divided by the air density value of 1.29 to give the value of $Mass_{reacted}$ in Litre/minute unit. The air stoichiometry $?_{air}$ then can be found by dividing $Mass_{flow}$ to $Mass_{reacted}$ (6.84 × 10^{-2} /62.2 ×10^{-3} ? 1). The values of $?_{air}$ = 10, 20, and 30 was calculated similarly representing an average measured air velocity values of 0.75 m/s , 1.29 m/s, and 1.7 m/s respectively.

Figure 7 shows the accumulation of water in the cathode channels at an air stoichiometry of 1, 10, 20, and 30. The images were captured after 5, 10 and 15 minutes from the start of the AB-PEMFC operation. It is clear from Figure 7 that droplets were smaller in size and in less numbers for the natural free condition ($?_{air}$ = 1). No droplet was observed in the first 5 minutes of operation and the current density of the cell was at its lowest value (80 mA/cm^2) compared to other tested stoichiometry conditions (~140 mA/cm^2). At an air stoichiometry of 10 and 20, the size of the droplets became larger and the channels contained more water with a peak current density of 150 mA/cm^2. When $?_{air}$ increased to 30, the amount of water in the channels slightly reduced by the mass transport mechanism of the air flow but even at this high flow range water was not cleared from the channels.

The relative humidity of the air at the exit of one of the flow channels was measured by the humidity sensor (44% RH) and was found to be slightly higher than the ambient humidity value (40% RH) that was measured before AB-PEMFC operation. Although the humidity value of the exit air is expected to increase significantly due to the water produced by the reaction of the cell, but the effect of the heat generated from the cell (temperature increased by 25 C°) that travels upwards in the same direction of the exit air could be sufficient to evaporate the produced water and hence maintains the relative humidity value largely unchanged.

Effect of hydrogen stoichiometry

The hydrogen stoichiometry $?_{H2}$ was calculated at a similar current density value to that of air (at 150mA/cm^2). Figure 8 shows the accumulation of water under four different hydrogen stoichiometry conditions ($?_{H2}$) 0.4, 0.8, 1.25, and 1.66. No droplet was produced in the first 5 minutes of operation when $?_{H2}$= 0.4. Droplets started to appear on the surface at a later stage but in moderate quantity and at low current density values (~100 mA/cm^2). At $?_{H2}$= 1.25, the cell produced the maximum amount of water in the channels and achieved a peak current density of 147.6 mA/cm^2. It can be seen from Figure 8 that at $?_{H2}$= 0.8 a water film was developed on the side wall of the channel which tended to agitate downwards in the gravitational direction of the cell. Another water film was also observed at $?_{H2}$= 1.25 but it drained away immediately from the channel once merged with the surrounding droplets. This phenomenon probably occurred due to the increase in the weight of the water film which rises the effect of gravitational force over the film adhesive force with the GDL surface and the channel land. As $?_{H2}$ increased to 1.66, the number of droplets in the channels reduced gradually with time. The current density of the cell also reduced to 143 mA/cm^2 due to membrane dehydration on the anode side.

?$_{air}$ = 1/ I_{cell} =80 mA.cm^{-2} **?$_{air}$ = 1/ I_{cell} =80.2 mA.cm^{-2}** **?$_{air}$ = 1/ I_{cell} =80.3 mA.cm^{-2}**

?$_{air}$ = 10/ I_{cell} =150 mA.cm^{-2} **?$_{air}$ = 10/ I_{cell}=150.1 mA.cm^{-2}** **?$_{air}$ = 10/ I_{cell}=150.1 mAcm^{-2}**

=145.2 mAcm^{-2}

?$_{air}$ = 30/ I_{cell}=142.5 mA.cm^{-2} **?$_{air}$ = 30/ I_{cell}=142.6 mA.cm^{-2}** **?$_{air}$ = 30/ I_{cell}=142.5 mA.cm^{-2}**

Figure 7 Water accumulation under different air stoichiometry and operating times

?$_{H2}$ = 0.4/ I_{cell}=100 mA.cm^{-2} **?$_{H2}$ = 0.4/ I_{cell}=100.1 mA.cm^{-2}** **?$_{H2}$ = 0.4/ I_{cell}=100 mA.cm^{-2}**

?$_{H2}$ = 0.8/ I_{cell}=124 mA.cm^{-2} **?$_{H2}$ = 0.8/ I_{cell}=124.4 mA.cm^{-2}** **?$_{H2}$ = 0.8/ I_{cell}=124.6 mA.cm^{-2}**

$?_{H2}$ = 1.25/ I_{cell}=147.6 mA.cm^{-2} $?_{H2}$ = 1.25/ I_{cell}=147.4 mA.cm^{-2} $?_{H2}$ = 1.25/ I_{cell}=147.5 mA.cm^{-2}

$?_{H2}$=1.66/ I_{cell}=143.1 mA.cm^{-} $?_{H2}$

Figure 8 Water accumulation under different hydrogen stoichiometry and operating times

Effect of cell temperature

The cell was heated at the anode flow plate up to a temperature of 60 C° to examine the effect of the operating temperature on the evaporation of water droplets in the cathode channels as well as on the current density of the cell. Figure 9 shows images in the channels at cell temperatures of 40°, 50°, and 60 C°. It is clear that water droplets evaporate significantly with increasing temperature above the ambient room temperature (~23 C°). Few droplets were found in the channels when operating at 50 C° but all evaporated when the temperature reached 60 C°. The obtained current density values at those temperatures suggest that increasing the cell temperature reduces the internal resistance of the cell but it can be argued that also too much heat can cause the membrane to dehydrate and its conductivity to reduce.

Effect of external load

Figure 10 shows images of water accumulation in the channels for three time intervals (5, 10, 15 min) and under different load conditions (R= 0.11, 0.15, 0.32, 0.57 ?). It can be seen from these images that droplets start to appear in the channels after 5min of operation and develop further in size with operating time. No water was observed in the channels when the load reached 0.57 ?. This is likely to be due to the reduction of the current density (reduced ~117 mA/cm^2 from 0.11 to 0.57 ?) which is directly associated to the amount of water produced by the electrochemical reaction. At this point the water removal rate caused by the air flow was sufficient to extract all water produced from the channels. However, this was not the case when the load was at 0.11, 0.15, and 0.32 ?. Droplets aggregation in the channels becomes less as the load increases from 0.11 to 0.32 ? making the effect of water extraction rate from the channels more conspicuous. The images also show water film developed on the side wall of the channel at R = 0.11?, 0.15 ? which became larger in size when the load increased to 0.32 ?. This size enlargement which occurred noticeably at reduced current density value (~96 mA/cm^2) maybe caused by the coalescence of local droplets that appeared to be absent from the images.

T = 30 C°/ I_{cell}=150 mA.cm^{-2} **T = 30 C°/ I_{cell}=150.1 mA.cm^{-2}** **T = 30 C°/ I_{cell}=150.2 mA.cm^{-2}**

T = 40 C°/ I_{cell}=154 mA.cm^{-2} **T = 40 C°/ I_{cell}=154.2 mA.cm^{-2}** **T = 40 C°/ I_{cell}=154.2 mA.cm^{-2}**

T = 50 C°/ I_{cell}=152 mA.cm^{-2} **T = 50 C°/ I_{cell}=152.1 mA.cm^{-2}** **T = 50 C°/ I_{cell}=152.1 mA.cm^{-2}**

T = 60 C°/I_{cell}=140.2 mA.cm^{-2} **T = 60 C°/ I_{cell}=140 mA.cm^{-2}** **T = 60 C°/ I_{cell}=140 mA.cm^{-2}**

Figure 9 Water accumulation under different cell temperatures and operating times

R = 0.11 ?/ I_{cell}=146.8 mA.cm^{-2} **R = 0.11 ?/ I_{cell}=146 mA.cm^{-2}** **R = 0.11 ?/ I_{cell}=146 mA.cm^{-2}**

R=0.15 ?/ I_{cell} =106.5 mA.cm^{-2} **R=0.15 ?/ I_{cell}=106.4 mA.cm^{-2}** **R=0.15 ?/ I_{cell}=106.4 mA.cm^{-2}**

R=0.32 ?/ I_{cell}=50 mA.cm^{-2} **R=0.32 ?/ I_{cell}=50.2 mA.cm^{-2}** **R=0.32 ? / I_{cell}=50.2 mA.cm^{-2}**

R=0.57 ?/ I_{cell}=29.7 mA.cm^{-2} **R=0.57 ?/ I_{cell} =29.6 mA.cm^{-2}** **R=0.57 ?/ I_{cell}=29.6 mA.cm^{-2}**

Figure 10 Water accumulation under different loads and operating times

4. Conclusions

The accumulation of water droplets in the cathode flow channels of air-breathing fuel cells was investigated by direct visualisation under various operating conditions. The optical system arrangement together with the transparent window which was incorporated into the cathode side of the cell have allowed simultaneous observation of the droplet formation on the surface of the membrane from the top and side views of the channels. The captured images revealed that during droplet formation their advancing and receding contact angles are almost equal. The contact angles and droplet heights increased with increasing droplet diameter, exhibiting a similar trend that reduces slightly at larger droplet diameters. Water films were able to develop and maintain direct contact with the side-wall of the channels even under the effect of gravitational force. The impact of air and hydrogen stiochiometry operating conditions was found to be strong on droplets aggregation in the channels but minimal on droplets extraction from the channels. In contrast, changes in the operating temperature proved to be the most effective water removal mechanism, with minimum reduction in the current density of the AB-PEMFC.

Table 1 Test operating conditions

Acknowledgement

The authors would like to acknowledge the support of Johnson Matthey Fuel Cell Group in providing Nafion membranes, also the support of the Energy and the Environment team at City University.

References

1. Buchmann I. Batteries in a Portable World — A Handbook on Rechargeable Batteries for Non-Engineers. Cadex Electronics Inc; 2nd Edition, 2001

2. Dyer CK. Fuel cells for portable applications. J Power Sources 2002; 106(1-2):31-34.

3. Hahn R., Wagner S., Krumbholz S., Reichl H. Optimization of efficiency and energy density of passive micro fuel cells and galvanic hydrogen generators. EDA Publishing Association - DTIP 2008; Symposium on Design, Test, Integration and Packaging of MEMS/MOEMS,

4. Han SK., Yeon HC., Miesse CM., Jang JH., Oh YS., Cha SW. Air-breathing miniature planar stack using

the flexible printed circuit board as a current collector. Int J Hydrogen Energy 2009; 34(1):459-466.

5. Akyalç?n L., Kaytako?lu S. Optimization of structural combinations on the performance of a PEMFC's MEA. J Power Sources 2008; 180(2):767-772.

6. Yang T., Shi P. A preliminary study of a six-cell stack with dead-end anode and open-slits cathode. Int J Hydrogen Energy 2008; 33(11):2795-2801

7. Spiegel CS., Agarwal R., Bhansali S. Comparison of microchannel dimensions for air-breathing polymer exchange membrane microfuel cells. J Power Sources 2008; 182(2):603-608

8. Chen CY., Lai WH., Weng BJ., Chuang HJ., Hsieh CY., Kung CC. Planar array stack design aided by rapid prototyping in development of air-breathing PEMFC. J Power Sources 2008; 179(1):147-154

9. Jaouen F., Haasl S., van der Wijngaart W., Lundblad A., Lindbergh G., Stemme G. Adhesive copper films for an air-breathing polymer electrolyte fuel cell. J Power Sources 2005; 144 (1):113-121

10. Jeong SU., Cho EA., Kim HJ., Lim TH., Oh IH., Kim SH. Effects of cathode open area and relative humidity on the performance of air-breathing polymer electrolyte membrane fuel cells. J Power Sources 2006; 158(1):348-353

11. Schmitz A., Tranitz M., Eccarius S., Weil A., Hebling C. Influence of cathode opening size and wetting properties of diffusion layers on the performance of air-breathing PEMFCs. J Power Sources 2006; 154(2):437-447

12. Santa Rosa DT., Pinto DG., Silva VS., Silva RA., Rangel CM. High performance PEMFC stack with open-cathode at ambient pressure and temperature conditions. Int J Hydrogen Energy 2007; 32(17):4350-4357

13. Zhang Y., Mawardi A., Pitchumani R. Numerical studies on an air-breathing proton exchange membrane (PEM) fuel cell stack. J Power Sources 2007; 173(1):264-276

14. Rajani BPM., Kolar AK. A model for a vertical planar air breathing PEM fuel cell. J Power Sources 2007; 164(1): 210-221

15. Ying w., Ke J., Lee WY., Yang TH., Kim CS. Effects of cathode channel configurations on the performance of an air-breathing PEMFC. Int J Hydrogen Energy 2005; 30(12):1351-1361

16. Ying W., Yang TH., Lee WY., Ke J., Kim CS. Three-dimensional analysis for effect of channel configuration on the performance of a small air-breathing proton exchange membrane fuel cell (PEMFC). J Power Sources 2005; 145(2):572-581

17. Chu D., Jiang R., Performance of polymer electrolyte membrane fuel cell (PEMFC) stacks: Part I. Evaluation and simulation of an air-breathing PEMFC stack. J Power Sources 1999; 83(1-2):128-133

18. Zhang Y., Pitchumani R. Numerical studies on an air-breathing proton exchange membrane (PEM) fuel cell. Int J Heat and Mass Transfer 2007; 50(23-24):4698-4712

19. Yalcinoz T., Alam MS. Dynamic modeling and simulation of air-breathing proton exchange membrane fuel cell. J Power Sources 2008; 182(1): 168-174

20. Ying W., Sohn YJ., Lee WY., Ke J., Kim CS. Three-dimensional modeling and experimental investigation for an air-breathing polymer electrolyte membrane fuel cell (PEMFC). J Power Sources 2005; 145(2):563-571

21. Litster S., Djilali N., Mathematical modelling of ambient air-breathing fuel cells for portable devices. Electrochimica Acta 2007; 52(11): 3849-3862

22. Wang Y., Ouyang M. Three-dimensional heat and mass transfer analysis in an air-breathing proton exchange membrane fuel cell. J Power Sources 2007; 164(2): 721-729

23. Hwang JJ., Wu SD., Pen RG., Chen PY., Chao CH. Mass/electron co-transports in an air-breathing cathode of a PEM fuel cell. J Power Sources 2006; 160(1):18-26

24. Hwang JJ., Chao CH. Species-electrochemical transports in a free-breathing cathode of a PCB-based fuel cell. Electrochimica Acta 2007; 52(5):1942-1950

25. Litster S., Djilali N. Mathematical modelling of ambient air-breathing fuel cells for portable devices. Electrochimica Acta 2007; 52(11): 3849-3862

26. O'Hayre R., Fabian T., Litster S., Prinz FB., Santiago JG. Engineering model of a passive planar air breathing fuel cell cathode. J Power Sources 2007; 167(1): 118-129

27. Jeong SU., Cho EA., Kim HJ., Lim TH., Oh IH., Kim SH. A study on cathode structure and water transport in air-breathing PEM fuel cells. J Power Sources 2006; 159(2):1089-1094

28. Jung UH., Jeong SU., Park KT., Lee HM., Chun K., Choi DW., Kim SH. Improvement of water management in air-breathing and air-blowing PEMFC at low temperature using hydrophilic silica nano-particles. Int J Hydrogen Energy 2007; 32(17):4459-4465

29. Paquin M., Fréchette LG. Understanding cathode flooding and dry-out for water management in air breathing PEM fuel cells. J Power Sources 2008: 180(1) 440-451

30. Fabian T., Posner JD., O'Hayre R., Cha SW., Eaton JK., Prinz FB., Santiago JG. The role of ambient conditions on the performance of a planar, air-breathing hydrogen PEM fuel cell. J Power Sources 2006; 161(1):168-182

31. Ous T., Arcoumanis C. Visualisation of water droplets during the operation of PEM fuel cells. J Power Sources 2007; 173(1):137-148

Air Fan

Fuel Cell Unit (FCU)

Hydrogen Unit

Control Unit

Monitoring
Unit

hot wire probe positioned at

left wall

centre

right wall

Air channel exit

End-plate anode

Hot wire probe

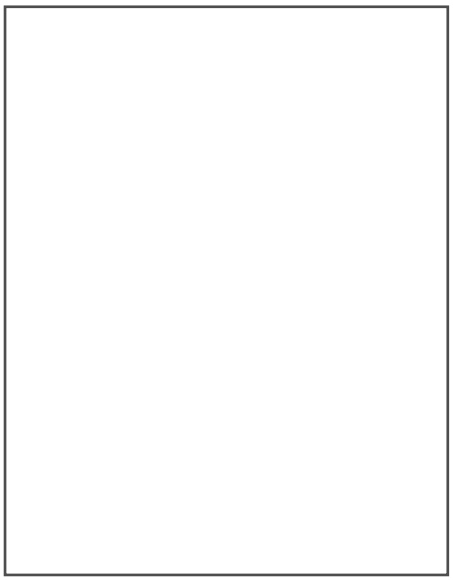

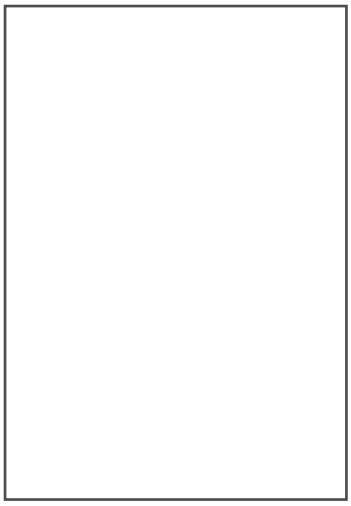

Flow channels

Land

Land bridges

Machined through area

Transparent window

Heating plate

Cathode flow plate design

End-plate cathode

Cathode end-plate

Anode end-plate

Anode flow plate

Cathode flow plate

MEA

Heating plate

Plexiglass plate

FCU base

FCU

Transparent window

Cathode flow plate

SensiCam

Spindle

Position controller

Camera 1

Vertical supporting base

SensiCam

Position
controller

Camera 2

Visualisation platform

Spindle

Horizontal observation

Vertical observation

Time synchronisation

Screen 1

Screen 2

Land

Land

Channel

Droplets

Droplets

Membrane

Droplet 1 top view

Droplet 1 side view

1.1 mm

0.7 mm

0.7mm

0.7mm

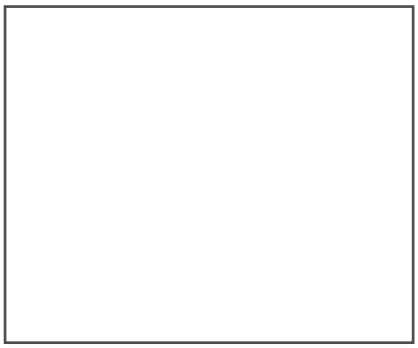

Membrane

Droplet merging with carbon fibre

Droplet reaching maximum size

0.7 mm

0.7 mm

Operating time 6 min

Operating time 5.30 min

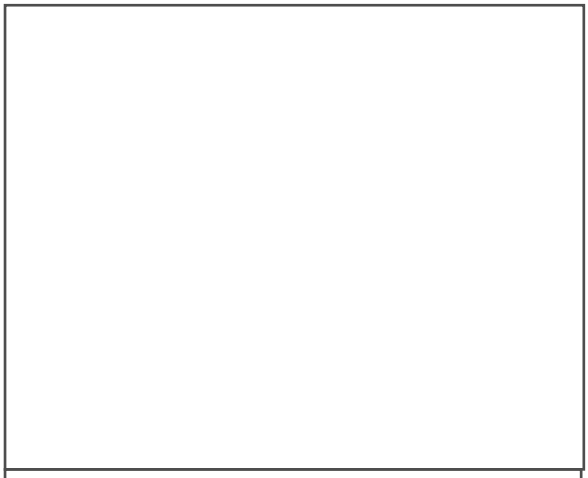

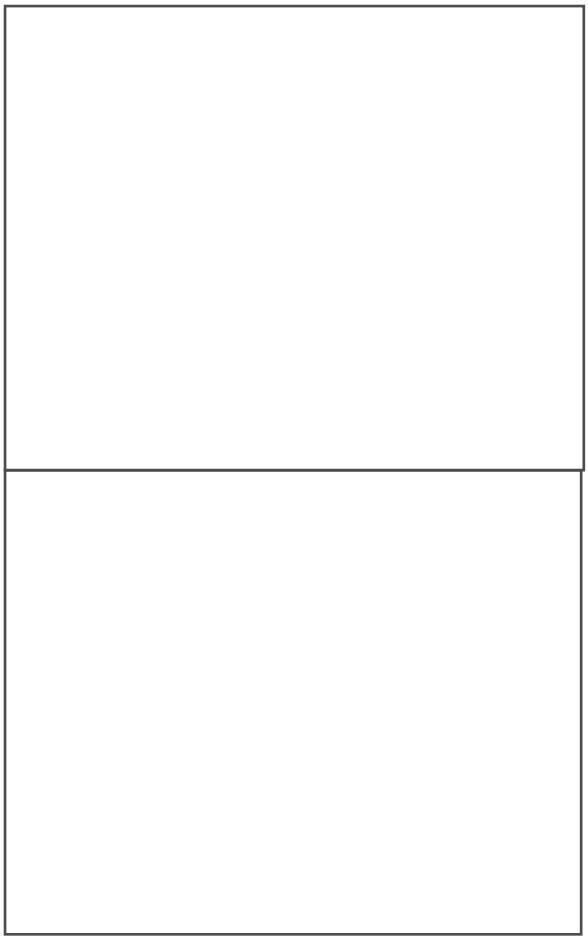

d = 288 µm, h = 250 µm, contact angle = 135.7°

d = 290 µm, h = 258 mm, contact angle = 138.5°

Operating time 7 min

Operating time 6.30 min

d = 305 µm, h = 268 µm, contact angle = 140.7°

d = 314 µm, h = 274 µm, contact angle = 142.6°

Operating time 8 min

Operating time 7.30 min

d = 320 µm, h = 277act angle = 142.6°

Operating time 8 min

Operating time 7.30 min

d = 320 µm, h = 277 µm, contact angle = 144°

d = 329 µm, h = 283 µm, contact angle = 146°

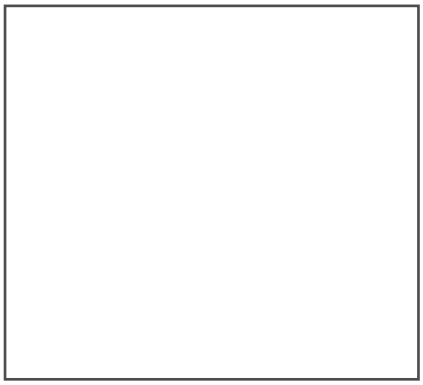

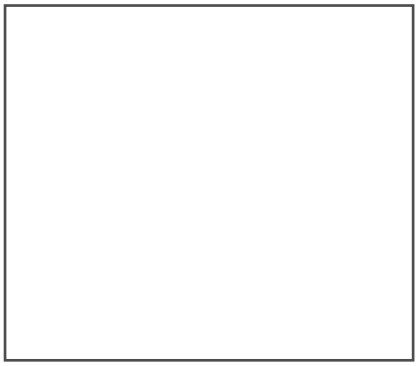

?air = 1/ Icell =80 mA.cm-2 ?air = 1/ Icell =80.2 mA.cm-2 ?air = 1/ Icell =80.3 mA.cm-2

?air = 10/ Icell =150 mA.cm-2 ?air = 10/ Icell=150.1 mA.cm-2 ?air = 10/ Icell=150.1 mAcm-2

?air = 20/ Icell=145 mA.cm-2 ?air = 20/ Icell=145.3 mA.cm-2 ?air = 20/ Icell=145.2 mAcm-2

?air = 30/ Icell=142.5 mA.cm-2 ?air = 30/ Icell=142.6 mA.cm-2 ?air = 30/ Icell=142.5 mA.cm-2

Land

t = 15 min

t = 5 min

t = 10 min

Air-flow

Channel width 5 mm

t = 15 min

t = 10 min

t = 5 min

t = 15 min

t = 10 min

t = 5 min

t = 15 min

t = 10 min

t = 5 min

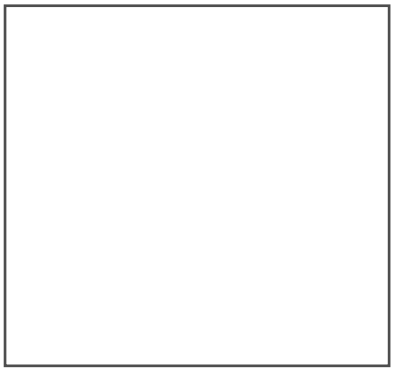

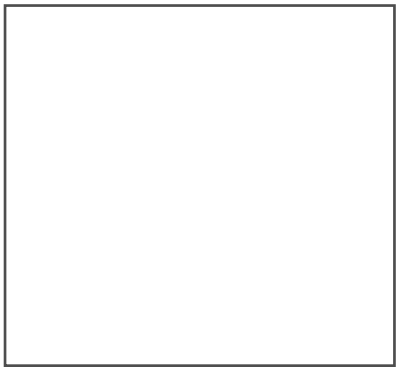

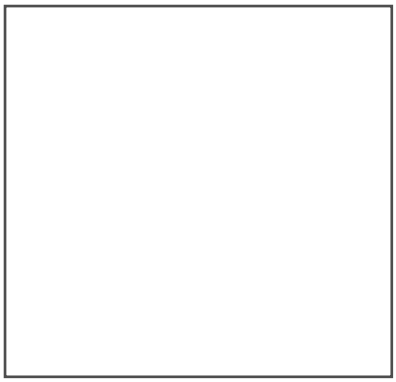

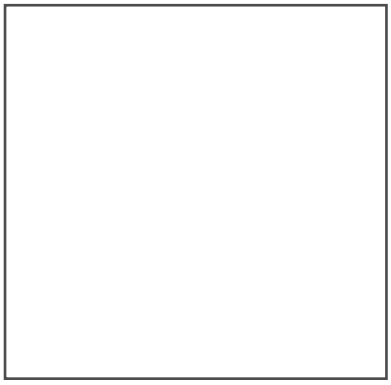

?H2 = 0.4/ Icell=100 mA.cm-2 ?H2 = 0.4/ Icell=100.1 mA.cm-2 ?H2 = 0.4/ Icell=100 mA.cm-2

?H2 = 0.8/ Icell=124 mA.cm-2 ?H2 = 0.8/ Icell=124.4 mA.cm-2 ?H2 = 0.8/ Icell=124.6 mA.cm-2

?H2 = 1.25/ Icell=147.6 mA.cm-2 ?H2 = 1.25/ Icell=147.4 mA.cm-2 ?H2 = 1.25/ Icell=147.5 mA.cm-2

?H2=1.66/ Icell=143.1 mA.cm-2 ?H2 = 1.66/ Icell=143 mA/ cm2 ?H2 = 1.66/ Icell=143 mA.cm-2

t = 15 min

t = 5 min

t = 10 min

t = 15 min

t = 5 min

t = 10 min

t = 15 min

t = 10 min

t = 5 min

t = 5 min

t = 10 min

t = 15 min

t = 15 min

t = 5 min

t = 10 min

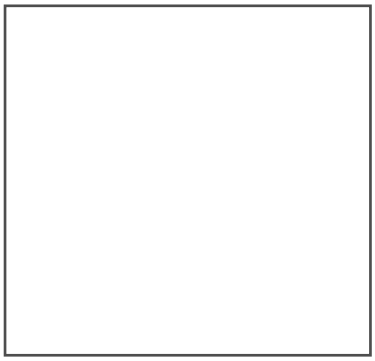

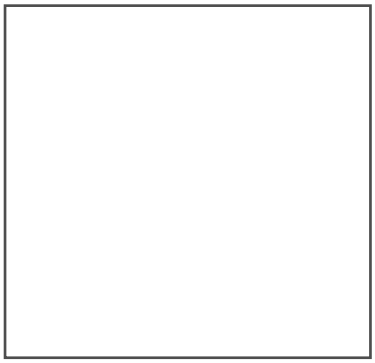

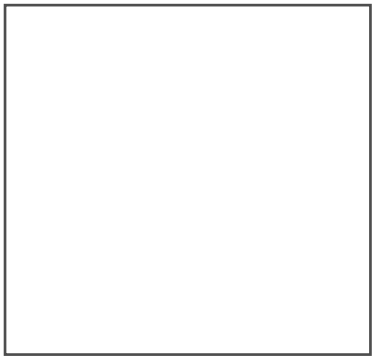

t = 15 min

t = 5 min

t = 10 min

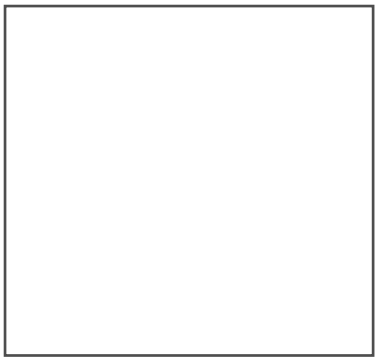

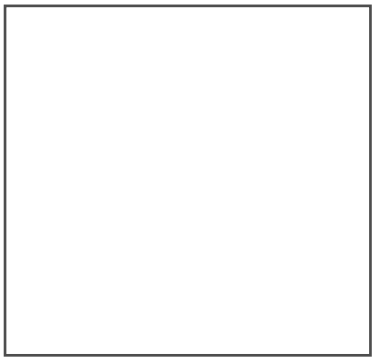

t = 15 min

t = 5 min

t = 10 min

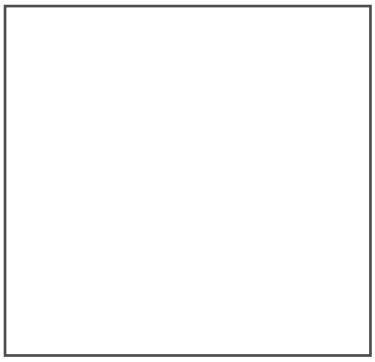

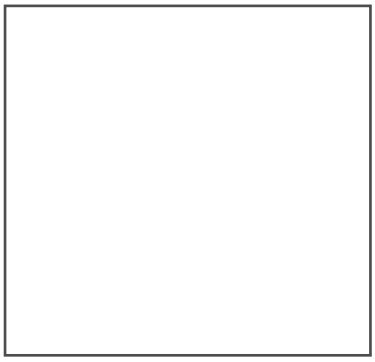

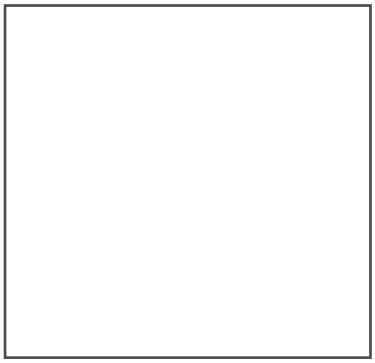

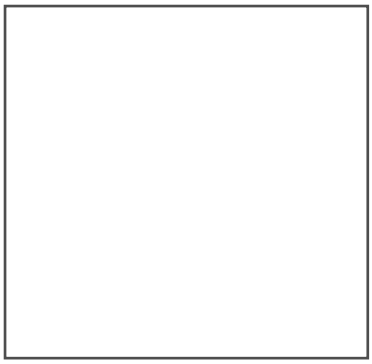

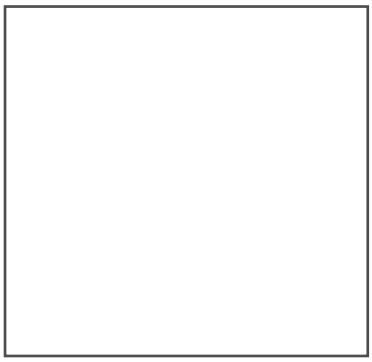

t = 15 min

t = 5 min

t = 10 min

t = 15 min

t = 5 min

t = 10 min

R = 0.11 ?/ Icell=146.8 mA.cm-2 R = 0.11 ?/ Icell=146 mA.cm-2 R = 0.11 ?/ Icell=146 mA.cm-2

R=0.15 ?/ Icell =106.5 mA.cm-2 R=0.15 ?/ Icell=106.4 mA.cm-2 R=0.15 ?/ Icell=106.4 mA.cm-2

R=0.32 ?/ Icell=50 mA.cm-2 R=0.32 ?/ Icell=50.2 mA.cm-2 R=0.32 ? / Icell=50.2 mA.cm-2

t = 15 min

t = 5 min

t = 10 min

R=0.57 ?/ Icell=29.7 mA.cm-2 R=0.57 ?/ Icell =29.6 mA.cm-2 R=0.57 ?/ Icell=29.6 mA.cm-2

t = 15 min

t = 5 min

t = 10 min

t = 15 min

t = 5 min

t = 10 min

Exper no

1

2

3

4

5

Air Stoichiometry (?air)

4

variable

4

4

4

H2 Stoichiometry (?H2)

1.25

1.25

variable

0.6

0.6

Cell Temperature (C°)

23

23

23

variable

23

Load
(?)

0.11

0.11

0.11

0.11

variable